phys. stat. sol. (a) **166**, 327 (1998)

Subject classification: 61.85.+p; 61.16.Ch; 68.35.Ct; S10.1; S10.15

Atomic Column Resolved Electron Energy-Loss Spectroscopy

G. Duscher (a, b), N. D. Browning (b), and S. J. Pennycook (a)

(a) Oak Ridge National Laboratory, Bethel Valley Rd., Oak Ridge, TN 37831–6031, USA

(b) University of Illinois at Chicago, Chicago, Il, USA

(Received January 6, 1998)

Dedicated to Professor Dr. Manfred Rühle on the occasion of his 60th birthday

Spatially resolved electron energy-loss spectroscopy (EELS) is rapidly developing into a unique and powerful tool to characterize internal interfaces. Because atomic column resolved Z-contrast imaging can be performed simultaneously with EELS in the scanning transmission electron microscope, this combination allows the atomic structure to be correlated with the electronic structure, and thus the local properties of interfaces or defects can be determined directly. However, the ability to characterize interfaces and defects at that level requires not only high spatial resolution but also the exact knowledge of the beam location, from where the spectrum is obtained. Here we discuss several examples progressing from cases where the limitation in spatial resolution is given by the microscopes or the nature of the sample, to one example of impurity atoms at a grain boundary, which show intensity and fine structure changes from atomic column to atomic column. Such data can be interpreted as changes in valence of the impurity, depending on its exact site in the boundary plane. Analysis of this nature is a valuable first step in understanding the macroscopic structural, optical and electronic properties of materials.

1. Introduction

The ultimate resolution in electron energy-loss spectroscopy (EELS) performed in a transmission electron microscope is defined by two factors; the physical limit is set by the spatial extent of the interaction between the excited atom and the fast electron (impact parameter), while the diameter of the electron beam (probe) adds an instrumental limitation. Quantum mechanical treatments of the impact parameter give localization of the scattering event for higher losses below 0.1 nm (>100 eV for 100 kV incident energy [1]), see Fig. 1. Although, this is much broader than the width of the object function for Z-contrast imaging, for most practical purposes the dominating factor controlling spatial resolution in EELS remains therefore the probe diameter. There are two components that define the effective probe diameter; the first is the size of the incident beam and the second is the broadening of the beam in the specimen. The first component is defined by the microscope, while the thickness of an amorphous or off-axis crystalline sample controls the second one. However the study of crystalline specimens in low-order zone-axis orientations [2], [3] preserves the probe diameter within the specimen due to channeling. Thus the spatial resolution of the energy-loss measurements under channeling conditions is again defined by the incident probe.

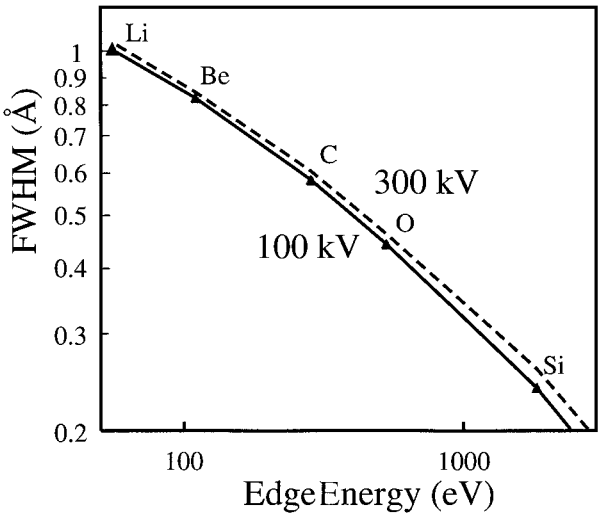

Fig. 1. The FWHM of the object functions for 100 kV and 300 kV incident electrons for K-loss excitation of various elements shows a localization of the inelastic scattering process below 0.1 nm

The ability to form electron probes with diameters comparable to the lattice parameter of many crystalline materials has been available in commercial instruments for almost ten years [4]. In the VG HB501 UX dedicated STEM, an optimum probe size of 0.22 nm full width at half maximum (FWHM) is routinely achieved. The small probe size in combination with a high angle annular dark field detector (HAADF) [3, 4], allows the acquisition of an incoherent image at atomic resolution, called a Z-contrast image, because the detected electrons are to first order Rutherford scattered and therefore the intensity is proportional to the mean square atomic number Z in the probed volume. In this microscope, the cold field emission source provides enough signal to perform Z-contrast imaging with atomic resolution and EELS analysis under the same conditions [5], [6].

However, although the capability is there to achieve atomic resolution EELS, it has been questioned why EELS at this level is not commonplace [7]. In fact, there is only one example in the literature where a spatial resolution lower than 0.5 nm is demonstrated with EELS [5]. There are several reasons why the resolution available in the instruments has not yet been fully exploited. In this paper we discuss the application of EELS to several materials to identify the limitations imposed on resolution by other additional factors, such as the nature of the specimen. We progress from examples where the specimens limit the obtainable spatial resolution to a case where the spatial resolution is limited by the instrument only. There, composition and valence states of impurity atoms at a grain boundary were obtainable with atomic column resolution.

2. Experimental Considerations

The instrument used for all the results presented in this paper is the VG HB501 UX dedicated STEM, operating at 100 kV and having an optimum probe diameter of 0.22 nm. The spectrometer/detection system follows the same basic principles as all currently available parallel detection systems for EELS in TEM/STEM [8]. The original magnetic sector prism serial spectrometer supplied by VG was modified by McMullan [9]. Here two quadrupoles were added at the exit slit of the spectrometer to magnify and project the energy dispersive plane onto a YAG scintillator. The so formed image on the scintil-

lator is optically coupled to an efficient multi-phase pinned CCD camera. The aim in using this CCD camera is to provide high efficiency for the low signal levels that are expected from the use of a small probe and the study of energy-losses above 100 eV. In fact, using this concept, single electron sensitivity is reached in the instrument used in this study [10]. The high detectum quantum efficiency (DQE) of the CCD means that the integration time for a single spectrum is only determined by the shot noise of the electrons. This allows acquisition times for most core edges of interest to be limited to 10 s. This is a crucial factor for atomic resolution EELS because longer exposer times limit not only the spatial resolution by instabilities of the microscopes but also enhance the possibility of sample damage.

To study the fine structure of the spectrum it is essential that the obtainable energy resolution is high. The cold field emission source in the VG HB501 UX enables us to achieve an energy resolution better than 0.8 eV, even with a collection aperture as large as 30 mrad. This aperture size is a compromise between signal levels and energy resolution. Using smaller collection apertures (e.g. 2 mrad) the intensity is much lower, but the energy resolution can be improved to 0.3 eV. For atomic resolution analysis this lower signal level increases the acquisition time and therefore reduces the spatial resolution due to microscope instabilities. There is also the question of how coherency and diffraction influences the intensity in the energy-loss spectrum. In a similar manner to the Z-contrast imaging technique, the use of the large detector integrates all of these effects guaranteeing incoherently generated spectra [1]. Additionally, large angle scattering events are more localized, which may enhance the resolution of the EELS. The expected resolution for a series of core losses is shown in Fig. 1, where large scattering angles are included.

In the system used, up to 100 spectra can be acquired consecutively and stored in the computer memory. Line scans were performed by scanning the beam continuously along a line, while spectra were continuously acquired and stored. During the acquisition of a spectrum the intensity of the HAADF detector can additionally be observed on an oscilloscope, which is especially helpful when the beam is scanned along a line or kept stationary and no image is displayed.

In order to obtain meaningful data the tendency of the sample to damage under the electron beam has to be explored. A time resolved acquisition of spectra with the same electron dose per atomic column, as in the spatially resolved experiment below, allows one to estimate the maximum acquisition time of a spectrum. If the sample does not allow acquisition of spectra while the beam is stationary at one atomic column, the dose can be reduced by scanning along a line parallel to a crystal plane. If even this is not possible the spatial difference technique is the only way to extract spatially resolved information, because the spectra are acquired while the beam is scanned in a rectangular area thereby reducing the electron dose. This technique is also of use if no atomic column resolved Z-contrast image can be obtained. Recording several spectra per analysed volume in all the above techniques is necessary not only to improve statistics by summation, but also to check possible electron damage of each analysed volume.

3. Experimental Results

3.1 Grain boundary in MgO

In our first example of spatially resolved EELS we discuss the results obtained from a 27° [001] tilt grain boundary in MgO. The Z-contrast images of this boundary [11] reveal

an atomic structure which does not coincide with the structure in pristine grain boundaries in MgO according to previous experimental [12] and theoretical results [13]. The Z-contrast images of the grain boundary here investigated showed increased intensity in particular atomic columns at the grain boundary, which suggested a heavier impurity atom may be segregated there. Also bond valence sum analysis [14], [15] indicated that some atoms at the grain boundary do not correspond with their formal valence. The chemical analysis of the vendor suggested two elements (Fe and Ca) as possible candidates to segregate at the grain boundary. Both Fe and Ca are readily accessible by EELS, allowing us to accurately quantify the presence of these elements at the grain boundary.

Unfortunately, the atomic column separation, 0.21 nm, in the common ⟨100⟩ axis of both grains adjacent to the grain boundary is just beyond the resolution of the VG

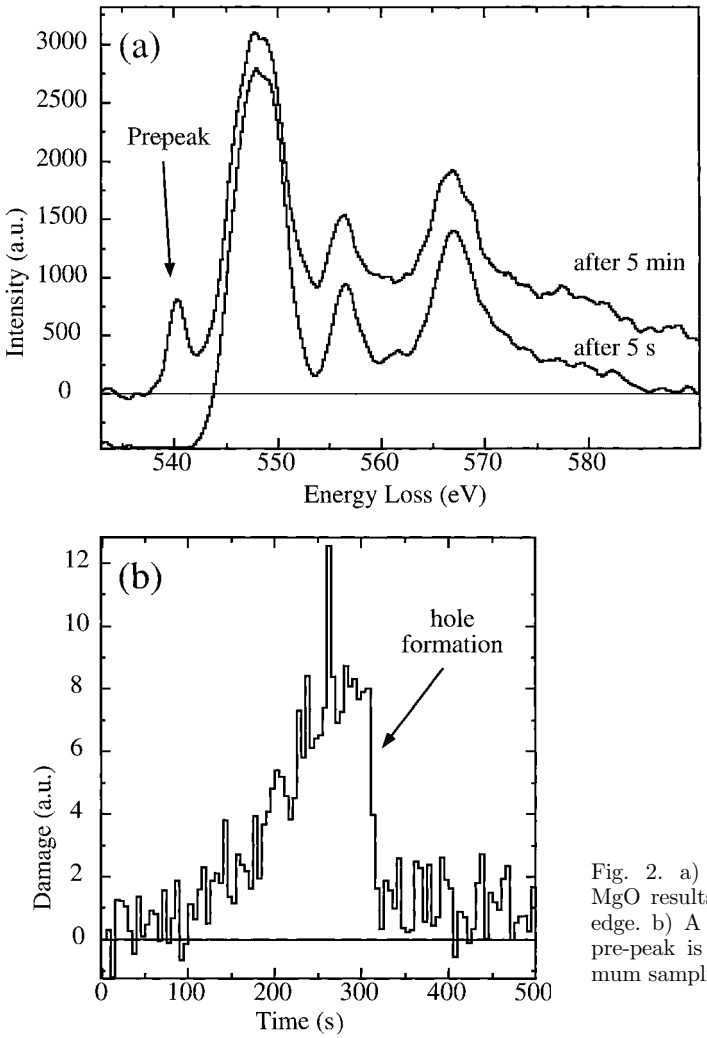

Fig. 2. a) Electron beam damage in MgO results in a pre-peak at the O−K edge. b) A plot of the intensity of this pre-peak is used to estimate the maximum sampling time before damage

HB501 UX. This makes direct atomic column resolved analysis impossible for this grain boundary. In addition, the sensitivity of this material to the 100 kV electron beam makes it unlikely that atomic column resolved EELS is possible at all in MgO. As an estimate of the time before beam damage occurs, a time sequence or chronospectroscopy [16] has been performed. A series of 100 spectra was acquired while the beam was continuously scanned in a 1 nm by 2 nm rectangle in the bulk region. Electron beam damage in MgO results in a pre-edge peak just below the onset of the oxygen-K ionization edge as shown in Fig. 2a. The area under this pre-peak, which is plotted in Fig. 2b, increases exponentially until the moment a hole is formed through the entire specimen. The appearance is consistent with the formation of O_2 molecules within the specimen, which can disappear after hole formation. The extrapolation of the curve in Fig. 2b leads to a maximum sampling time of 30 s. A stationary beam, resulting in a much higher dose, damages MgO instantaneously.

The difficulty in performing a direct atomic column resolved analysis leaves no choice but to use the spatial difference technique [17] in order to identify the segregated element. Ten spectra each with an integration time of 2 s were acquired while the beam was scanned over a 2 nm by 3 nm area with the grain boundary parallel to the longer axis of the scanned rectangle. The spectra were summed after acquisition to improve statistics. Another set of spectra was taken under the same conditions near the grain boundary to make changes in thickness minimal. This reference spectrum was used to subtract the background with less error, thereby giving higher compositional sensitivity [18].

The spatial difference spectrum in Fig. 3 shows clearly the presence of Ca at the grain boundary. The quantitative analysis resulted in an area density of about 3 Ca atoms per nm^2 of the grain boundary (approximately 0.2 monolayer), which is in the same order as estimated from the Z-contrast image [11]. No iron could be detected using this method.

As no atomic resolution analysis is possible in this MgO boundary, the sites of the calcium atoms could not be determined by spectroscopy. Also, as the fine structure of

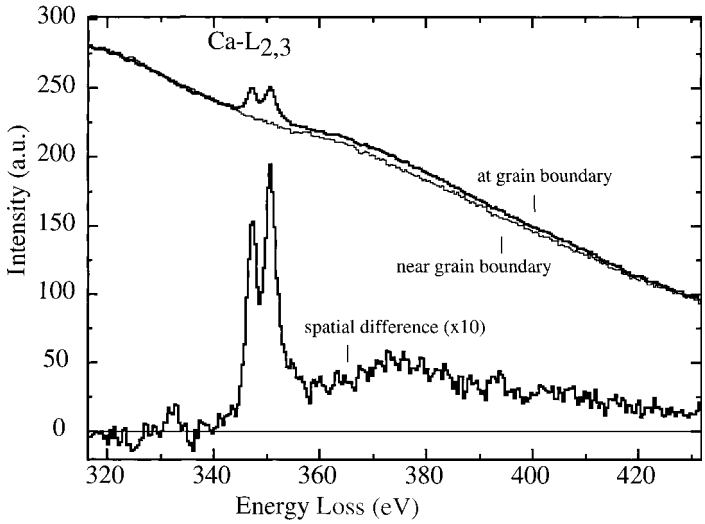

Fig. 3. The presence of the Ca-L edge is obvious in the EELS spectrum acquired from a 2 nm by 3 nm area containing a MgO grain boundary. The spectrum entirely from bulk material is used to determine the background under the Ca-L edge from the interface

the Ca-$L_{2,3}$ edge is not very sensitive to changes in coordination, bond lengths or angles to the oxygen nearest neighbors, no information on the Ca sites can be extracted from the spectrum. The analysis of the energy-loss near-edge structure of the Mg-$L_{2,3}$ edge and O-K edge in Fig. 4a, b do not show significant differences at the grain boundary compared to the bulk. Interpretation of the results at this level must therefore be confined to the suggestion that the coordination of Mg and O is very similar in the bulk and at the grain boundary.

One means to identify the preferred Ca sites at the grain boundary is through ab-initio calculations [19]. Plane wave pseudopotential calculations for this grain boundary have shown a high segregation energy for Ca in specific atomic sites seen bright in the Z-contrast image, and furthermore that the segregation induces a structural transformation [20].

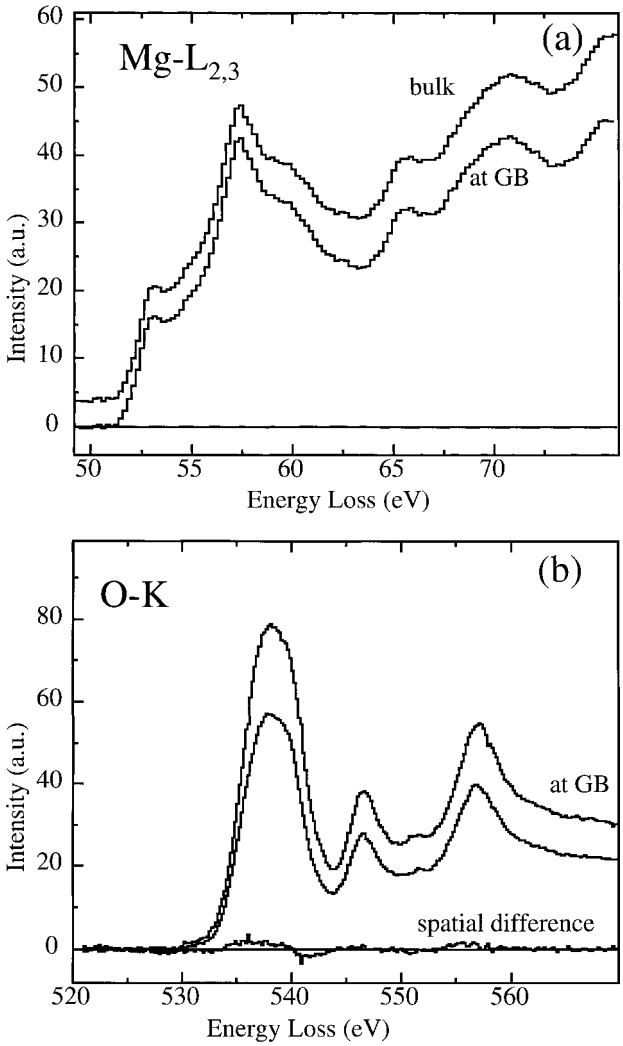

Fig. 4. The spatial difference of the Mg-$L_{2,3}$ (a) and O-K (b) confirms that there are no detectable changes in the ELNES of both edges at the grain boundary

3.2 BSCCO-tapes

Our second example of spatially resolved EELS concerns the analysis of grain boundaries in superconducting wires. Currently, the most developed material for power transmission application, $Bi_2Sr_2Ca_2Cu_3O_{7-\delta}$ (BSCCO 2223) cannot carry sufficient current for commercial applications. The reason for this is the microstructure, and in particular the grain boundaries that exist in the tape. In order to investigate detrimental influences of the grain boundaries on the superconducting properties of this material, we performed analytical studies on a sample showing low critical current characteristics.

While it is in principle possible to obtain a Z-contrast image from this material as shown in Fig. 5, no grain with the dominating phase of BSCCO 2223 was found in the right orientation. This highlights another difficulty in performing atomic resolution EELS in a dedicated STEM; a specimen tilt capacity limited to $\pm 10°$.

In this case, therefore, spectra were again acquired using the spatial difference technique, with the beam being scanned over a rectangular area of 2 nm by 3 nm. Spectra were obtained from the Cu-$L_{2,3}$ ionization edge, while the beam was scanned in a box containing the grain boundary or in the nearby area. Two of these spectra are shown in Fig. 6.

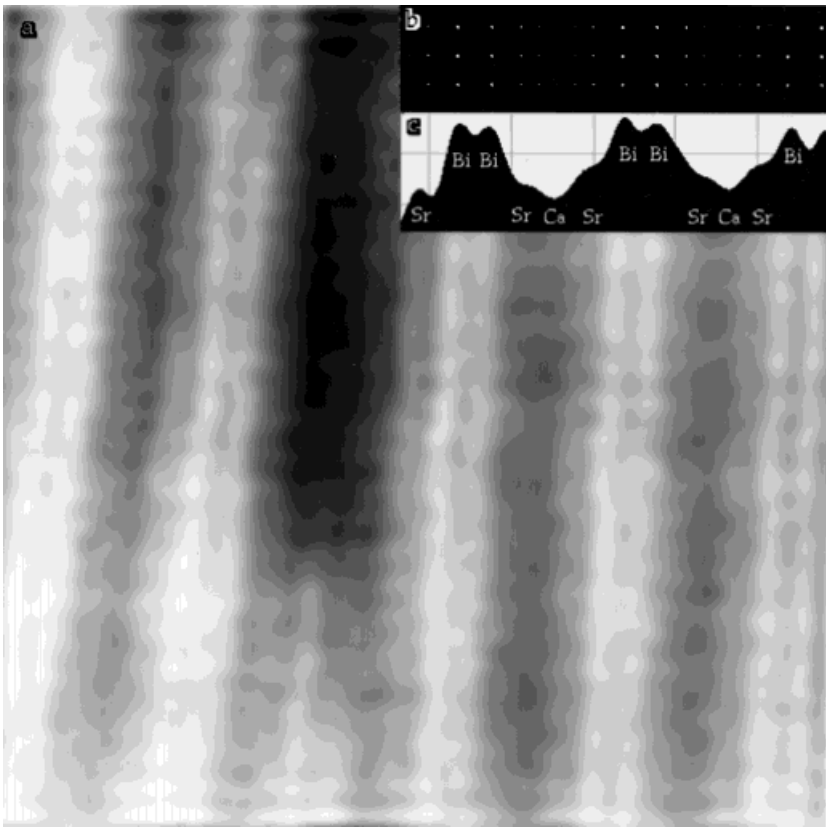

Fig. 5. a) Z-contrast image of a small angle grain boundary with adjacent Bi-2212 phase in BSCCO wires. The inset shows the ideal Z-contrast image (b) and a line-profile (c) of the actual image

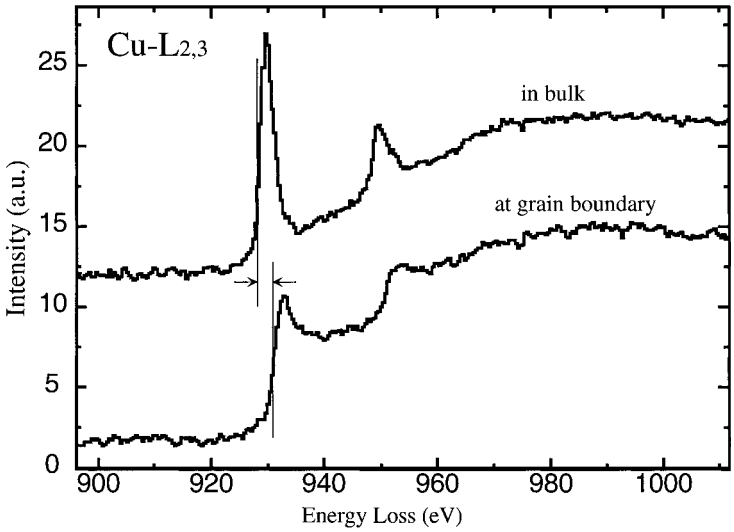

Fig. 6. Cu-L edge acquired at a Bi–BSCCO grain boundary and in the bulk. Cu with a lower oxidation state is present at the grain boundary, indicating a non-superconducting zone

The edge structure from the interface clearly shows a shift to higher energy and less pronounced peaks at the onsets (white lines) of both the L_3 and L_2 edges. The structure of the spectrum from the bulk material is similar to the reference spectrum of CuO, which shows the Cu valence of 2 or higher as expected in the superconducting phase. However the interface ELNES is comparable to the ELNES of Cu_2O. This shows a deficiency of the oxidation state of copper at the grain boundary, and therefore the material nearby cannot be a superconducting phase. The width of the area with copper of reduced

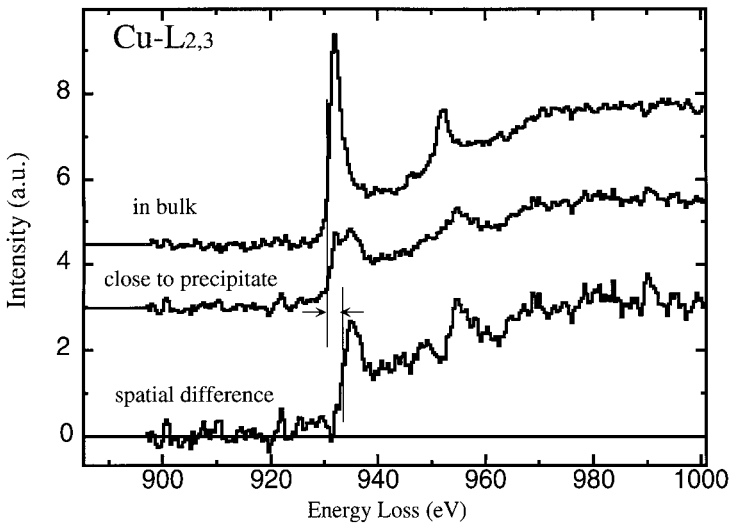

Fig. 7. Cu-L edge acquired near a lead oxide particle and in the bulk. Cu with a lower oxidation state is present close to this precipitate, as revealed by spatial difference

valence is obviously larger than 2 nm, the dimension of the scanned area perpendicular to the grain boundary, because no contribution of the bulk (superconducting) copper ELNES is visible. This extended non-superconducting area along the grain boundary can only act as a weak link junction and is therefore detrimental for superconductivity [21].

In the vicinity of lead oxide precipitates [21], which were easily located with Z-contrast imaging, the same reduced valence of Cu was found (Fig. 7). The depletion zone around these precipitates must be assumed spherical, and thus it is no surprise that contributions from the bulk are found in the spectra from this zone. The spatial difference technique reveals the same ELNES in the depletion zone around the precipitates as found at the grain boundaries. As these precipitates are mostly found near grain boundaries and are oxygen rich, we conclude that they also cause the oxygen deficiency zone elongated along the grain boundaries, which act as fast diffusion paths for oxygen. This conclusion is verified by an analysis of a higher critical current wire, where a significant decrease in the number of precipitates at grain boundaries was observed. A reduced copper oxidation state could not be found at the grain boundaries in that sample [21].

3.3 ZnTe nanoparticles

The third example of spatially resolved EELS involves the study of ZnTe nanoparticles grown by laser ablation and directly deposited on a holey carbon film. This new class of material has very promising characteristics for optoelectronic devices. Z-contrast and

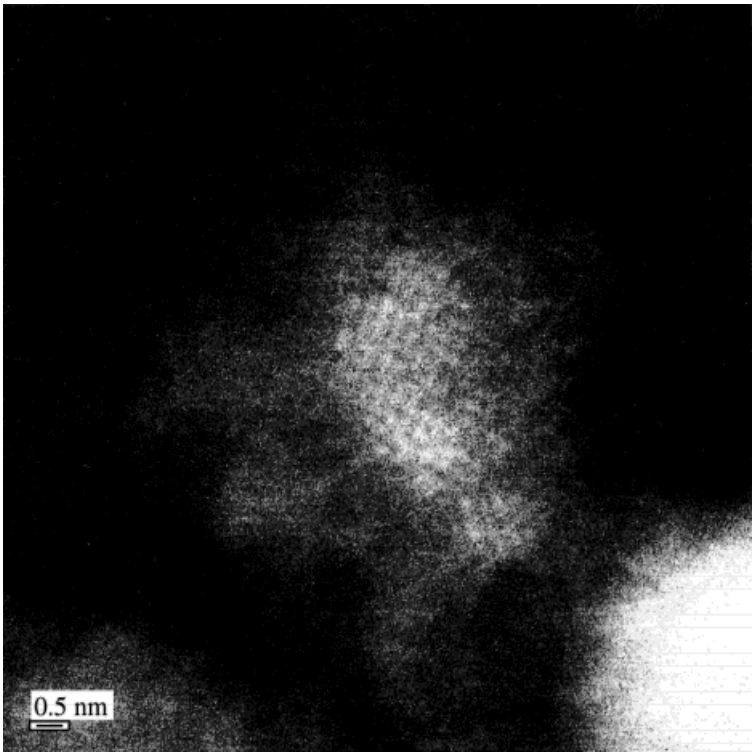

Fig. 8. Atomic column resolved Z-contrast image of ZnTe nanoparticles, showing a small particle joining a larger one, which contains two stacking faults

bright field STEM images show that nanoparticles produced in this manner are crystalline. However, the advantage of the Z-contrast image is immediately apparent: the higher Z of the particles compared to the holey carbon film they lay on, makes it possible to detect even small particles (<1 nm), even if they are not oriented along a major zone-axis. This is a significant difference from phase contrast high resolution transmission electron microscopy (HRTEM), where particles are identified by lattice fringes, and so only particles oriented close to a low order zone axis will be detected. In fact, it has been shown that it is even possible to identify individual atoms in this manner [22], [23].

The diameters of the particles observed lie in the range between 1 and 4 nm. All the particles contain a high density of stacking faults (as shown in Fig. 8), which may be one reason for their lack of luminescence. Another area of concern with these materials is the formation of a surface oxide layer and its effect on surface passivation. To investigate this we performed EELS linescans across the particles. In this case, the ability to observe an atomic resolution Z-contrast image confirms that the spatial resolution of the analysis is better than 0.3 nm.

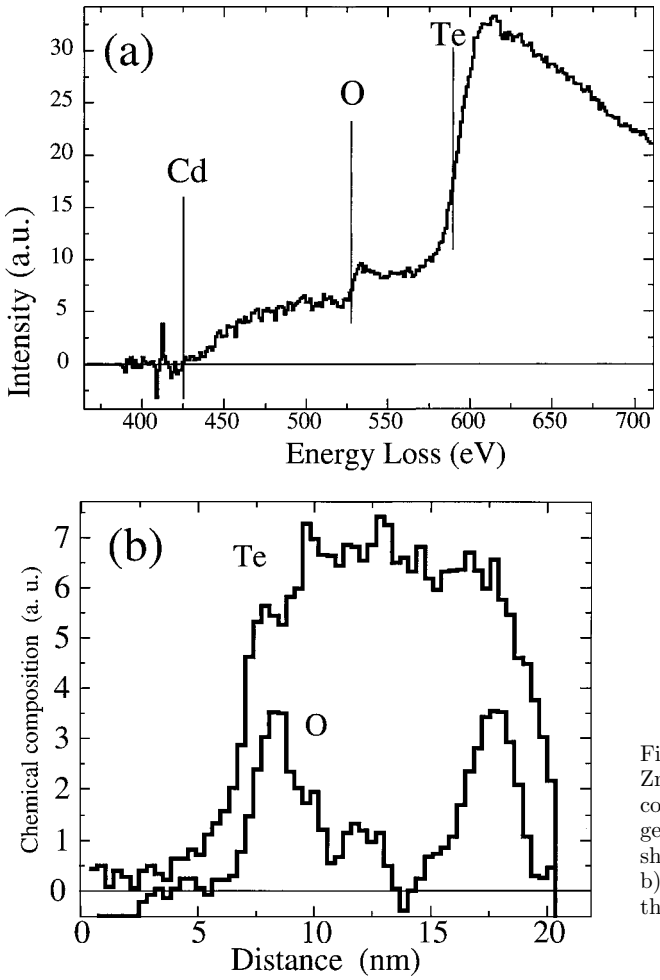

Fig. 9. a) A spectrum of the larger ZnTe nanoparticle shown in Fig. 8 contains also O and Cd. The oxygen is present as a surface oxide as shown in the chemical profile, b) calculated from a linescan across the same particle

The result of the linescan is shown in Fig. 9, where there is clear evidence of the shell-like structure of the oxide. The coincidence of the onset of the oxide with the Zn chemical profile suggests that there is zinc oxide at the surface. Quantitative analysis of the spectral intensity allows the surface layer to be estimated at 1 nm thick. Additionally, analysis of the particles by energy dispersive X-ray spectroscopy (EDS) located the presence of Cd and Se in the particles. The Cd could also be detected with EELS and the Cd is observed to be homogeneously distributed inside the nanoparticle, which is concluded from the fact that it shows the same chemical profile as Zn. Se was not observed in EELS analysis as the accessible edges are weak in intensity and show very few features. This makes quantitative analysis of some elements difficult with EELS and highlights an advantage in performing EDS in conjunction with EELS. The presence of Se and Cd, which are not detrimental for luminescence per se, was the result of material remaining from the earlier production of CdSe nanoparticles in the same chamber.

In this example, the Z-contrast image demonstrates that the beam diameter is of atomic dimensions and so theoretically atomic column resolved analysis should be possible. However, the small size of the particles is detrimental for that kind of analysis, as the particles roll under electron bombardment. Nevertheless, the chemical analysis together with the distribution of the elements and the direct observation of the particle structure, defect content and external facet structure by Z-contrast imaging reveals new insight into this new particle class. With a higher resolution STEM the combination of the techniques used here would also allow the determination of the surface terminations and three-dimensional structure of well faceted nanocrystals, such as are produced by chemical synthesis techniques.

3.4 Grain boundary in $SrTiO_3$

In our final example, we discuss the analysis of a $SrTiO_3$ bicrystal with a 36.7° ⟨100⟩ tilt grain boundary. This boundary has been deliberately doped with Mn, which has been

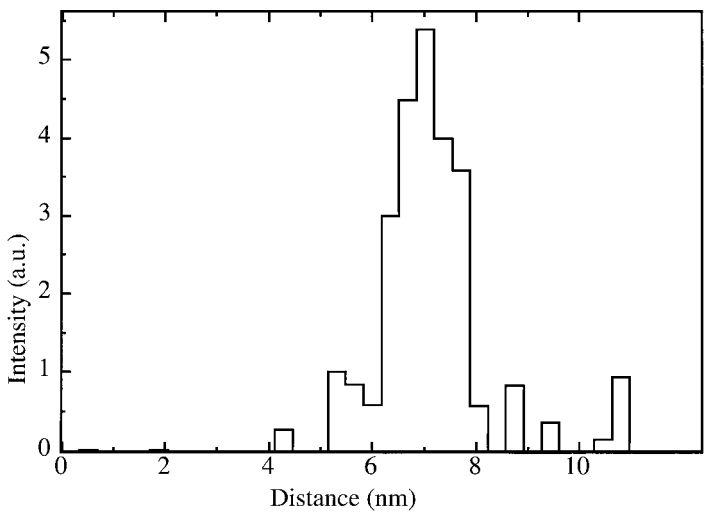

Fig. 10. The chemical profile as extracted from a linescan perpendicular to a $SrTiO_3$ grain boundary shows exctensive diffusion of Mn from the grain boundary into the bulk

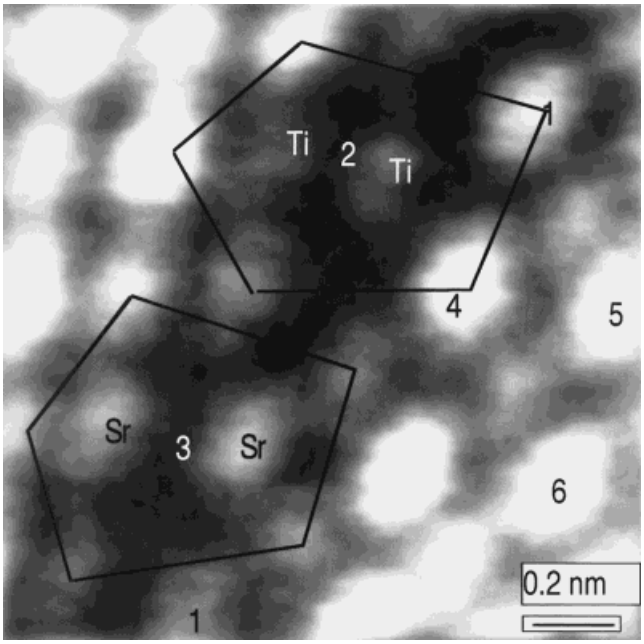

Fig. 11. The Z-contrast image of the Mn doped grain boundary shows the same structure as a pristine one. The structural units, which are similar to dislocation cores in $SrTiO_3$, and locations of the probe where spectra were taken, are indicated

diffused along the grain boundary into the bicrystal[24]. A chemical profile of Mn shows its distribution perpendicular to the grain boundary (Fig. 10). A high Mn content at the grain boundary is associated with a wide diffusion zone (>2 nm) into the bulk material.

The structure as observed in the Z-contrast image (Fig. 11) shows the same structure as reported from a pristine grain boundary [25]. The structure can be viewed as a series of structural units with the same atomic arrangements as found at dislocation cores in $SrTiO_3$, alternating between cation sublattices. Spacer units, equivalent to a distorted half unit cell, enable the transformation from one sublattice to the other. This model of the grain boundary is visualized in Fig. 11, which was acquired with a dedicated STEM VG HB603 U operated at 300 kV with an optimum probe size of 0.126 nm.

The spacing between the Sr and Ti atoms in this projection is 0.27 nm, which made it possible to obtain a Z-contrast image from the boundary core in the VG HB501 UX. However, the low intensity at the grain boundary, presumably caused by distortion due to Mn impurities or oxygen vacancies, meant that the Ti-columns at the core of the grain boundary could not be resolved with the VG HB501 UX, where the EELS analysis was performed.

Using this Z-contrast image as a guide, the electron probe was placed onto individual atomic columns for the acquisition of spectra. Before and after acquisition of a spectrum the position of the beam was checked on the image, while the HAADF intensity was monitored during spectrum acquisition on an oscilloscope. No sample drift could be detected during the acquisition of the five spectra at 3 s each. Thus the beam can be assumed to be centred on one atomic column, during the whole acquisition time.

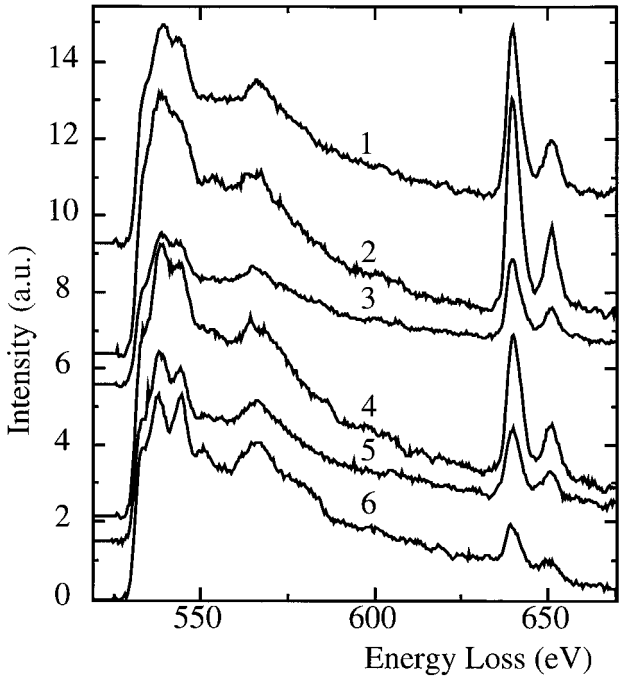

Fig. 12. The EELS spectra from the locations indicated in Fig. 11 after background subtraction show differences in the chemical content and the near edge structure from different atomic columns at the grain boundary

In the Z-contrast image, Fig. 11, the positions in the structure from which spectra were obtained are marked. These spectra (after subtracting the background prior to the O-K edge), containing both the O-K edge and the Mn-$L_{2,3}$ edge, are displayed in Fig. 12. Clearly visible are differences between the spectra from the grain boundary core (1, 2, 3, 4) and the adjacent undisturbed area (5, 6). These differences are not only obvious in the reduction of the amount of manganese, but also in the change of the ELNES of the O-K edge.

A comparison of these results to the reference spectra by Kurata and Colliex [26] reveals a similarity to Mn_2O_3 in the branching ratio between L_2 and L_3 intensity. This suggests that the valence state of the Mn in the boundary is close to 3+ (± 0.3), rather than the 2+ suggested earlier [24]. Further analysis of the data is underway to determine not only the changes of the oxygen coordination at different locations of the grain boundary, but also preferred segregation sites of manganese [27]. However, even at this early stage it is obvious that the Mn did not change the structure of the $SrTiO_3$ boundary, suggesting that the different valence of Mn from Ti reflects a reduced coordination, which is consistent with the distorted columns evident from Z-contrast image.

4. Discussion

These four different examples show very clearly that both the sample and microscope have to fulfil certain conditions to obtain atomic column resolution in EELS. The latter example shows clearly that in the case of the STEM one can approach the theoretical quantum mechanical limit for spatial resolution in EELS. So far such a capability has not been demonstrated in the TEM, because there the spatial resolution in the image is dominated by instrumental factors, in particular the spherical aberration of the objective

lens. The objective lens is before the sample in the STEM and therefore the chromatic aberration does not limit the spatial resolution in EELS [28]. In addition, EELS imaging techniques in TEM generally include only small scattering angles, when coherent effects in the energy filtered image can complicate interpretation.

The key to further application of the STEM techniques at atomic resolution, is of course the ability to obtain an atomic column resolved Z-contrast image simultaneously with the EELS spectrum. This image is the most convenient way to prove the resolution, to determine the position from which the spectrum is acquired and the stability of the microscope. The ability to obtain a Z-contrast image therefore represents a minimum requirement for atomic resolution EELS.

In addition, the sample must not damage easily under the electron beam. This is dependent on the damage mechanism in the material and therefore the incident energy of the electrons. It is possible that increasing the accelerating voltage to increase resolution may change the damage mechanism and allow atomic resolution analysis from materials such as MgO. It appears that electron beam damage will always provide a limit for spatially resolved analysis in certain materials.

Even if the material does not allow atomic column resolution the careful application of the spatial difference technique is a way to reveal the electronic structure locally, because the dose can be chosen to be below the damage threshold. However, the interpretation of spatial difference results requires to make a number of assumptions. First, it reveals only the difference of the average local density of states, whereas at a grain boundary for example there might be several different sites with different local electronic structure contributing to the difference spectrum. This problem can only be solved by assuming a particular model structure, with extensive fine-structure calculation for all different sites (as performed by e.g. Scheu et al. [29]). Second, due to noise in the spectrum, the weighted difference which has to be performed for a spatial difference spectrum may not have a unique solution; the decomposition into characteristic ELNES is therefore rather dependent on the subjective view of the experimentalist. Only a study which compares the spatial difference technique with an atomic column resolved analysis can illuminate the applicability of this technique.

In the current examples, the perovskite $SrTiO_3$ represents a sample where atomic resolution is favorable. The lattice parameter is sufficiently large to permit resolution in the Z-contrast image and the material does not damage quickly under the electron beam. Due to the exceptional stability of the microscope at the time, we were able to achieve atomic resolution. This is demonstrated in the drastic change in both chemical composition of Mn and oxygen ELNES from different columns at the grain boundary. This example also demonstrates another factor that needs to be considered. While the resolution in the Z-contrast image was better than 0.27 nm, this resolution does not mean that the analysed volume is a single atomic column. While we can distinguish the atomic columns with different chemical composition and ELNES, the probe tails contribute significantly to the volume analysed by EELS spectra. Although the Z-contrast resolution is better given by the FWHM of the probe, the total analysed volume in EELS is obviously given by the probe intensity profile, which is dependent on the defocus used. For a more local analysis it may be advantageous to degrade the image resolution somewhat, by using a less than optimum defocus to reduce the intensity in the probe tails [30].

However, it must also be remembered that the EELS object function is significantly broader than that for the Z-contrast imaging. We may consider the EELS analysis to be

done with an effective probe size, which is given by a convolution of the actual probe size with the object function (about 0.1 nm). The optimum probe size for Z-contrast imaging of 0.22 nm in the VG HB501 UX, must therefore be assumed to be effectively 0.25 nm in the case of EELS analysis. This is consistent with our observation that no significant differences are seen between the bulk Sr or Ti columns. Also it is assumed that the Mn is substituting for the Ti, although it can still can be detected when the probe is located at the Sr columns. Clear differences are seen with the probe on neighboring Sr columns, demonstrating atomic column resolved analysis.

5. Conclusion

In this study we discussed the limiting factors in obtaining atom column resolved EELS through several examples. Under the exceptional experimental conditions available in the analysis of $SrTiO_3$, it was possible to obtain spatial resolution in EELS close to the theoretical limit for the optimum focused beam and achieve an atom column resolved analysis. At the present time there are two immediate means to achieve improved resolution in EELS. The fitting of a parallel EELS system to the VG HB603 U in Oak Ridge and the improved STEM capabilities in the 200 kV TEM/STEM now commercially available, makes the level of resolution achieved in this study widely available. The advantage of the high brightness of the electron source (100 times greater than synchrotron X-ray sources) and its high coherence offer the ability not only to image structures, but also to accurately locate a probe to determine the local electronic structure of selected individual atomic columns. This represents a new level of material characterization. Coupled with recent advances in computational power, this exceptional data capability provides an appealing opportunity to obtain a fundamental understanding of all important interfacial properties including adhesion, embrittlement, electrical and optical activity.

Acknowledgments We thank our colleagues at ORNL, especially M. F. Chisholm, C. Prouteau, Y. Yan, and Y. Xin, for fruitful discussions, V. Dravid for providing the $SrTiO_3$ samples, and D. H. Lowndes and C. M. Rouleau for synthesing the ZnTe nanoparticles. This research was funded by the Division of Materials Sciences, U.S. DOE, under contract DE-AC05-96OR22464 with Lockheed Martin Energy Research Corporation, under grant number DE-GF02-96ER45610 and DOE 96ER45610 with University of Illinois at Chicago, and in part by an appointment to ORNL Postdoctoral Research Program administered jointly by ORISE and ORNL.

References

[1] S. J. Pennycook, in: Handbook of Microscopy, Eds. S. Amelinckx, G. Van Tendeloo, D. Van Dyck, and J. Van Landuyt, VCH Publishers, Weinheim 1997 (p. 595).
[2] J. Fertig and H. Rose, Optik **59**, 407 (1981).
[3] S. J. Pennycook and D. E. Jesson, Phys. Rev. Lett. **64**, 938 (1990).
[4] S. J. Pennycook and L. A. Boatner, Nature **336**, 565 (1988).
[5] N. D. Browning and S. J. Pennycook, Nature **366**, 143 (1993).
[6] P. E. Batson, Nature **366**, 727 (1993).
[7] M. Rühle, MPI für Metallforschung, Stuttgart, several private communications, 1991 to 1996.
[8] R. F. Egerton, Electron Energy-Loss Spectroscopy in the Electron Microscope, 2nd ed., Plenum Press, New York 1996.

[9] D. McMullan, J. M. Rodenburg, Y. Murooka, and A. J. McGibbon, Inst. Phys. Conf. Ser. **98**, 55 (1990).
[10] N. D. Browning and S. J. Pennycook, Microb. Anal. **2**, 81 (1993).
[11] Y. Yan, M. F. Chisholm, G. Duscher, and S. J. Pennycook, accepted by J. Electron Mic., 1997.
[12] T. Kizuka, M. Ijima, and N. Tanaka, Proc. Microscopy and Microanal. 674 (1996).
[13] D. J. Harris, G. W. Watson, and S. C. Parker, Phil. Mag. **A74**, 407 (1996).
[14] I. D. Brown and D. Altermatt, Acta Cryst. **B41** 244 (1985).
[15] D. Altermatt and I. D. Brown, Acta Cryst. **B41** 240 (1985).
[16] C. Colliex, M. Tence, E. Lefevre, C. Mory, H. Gu, D. Bouchet, and C. Jeanguillaume, Mikrochim. Acta **112**, 71 (1994).
[17] S. D. Berger and S. J. Pennycook, Nature **298**, 635 (1982).
[18] H. Müllejans and J. Bruley, J. Physique **3**, C7–2083 (1993).
[19] A. Maiti, M. F. Chisholm, S. J. Pennycook, and S. T. Pantelides, Phys. Rev. Lett. **77**, 1306 (1996).
[20] Y. Yan, M. F. Chisholm, G. Duscher, A. Maiti, S. J. Pennycook, and S. T. Pantelides, to be published.
[21] C. Prouteau, G. Duscher, N. D. Browning, and S. J. Pennycook, accepted by Physica C, 1997.
[22] M. S. Isaacson, D. Kopf, M. Ohtsuki, and M. Utlaut, Ultramicroscopy **4**, 101 (1979).
[23] P. D. Nellist and S. J. Pennycook, Science **413**, 274 (1996).
[24] V. Ravikumar, R. P. Rodrigues, and V. P. Dravid, J. Phys. D **29**, 1799 (1996).
[25] N. D. Browning, S. J. Pennycook, M. F. Chisholm, M. M. McGibbon, and A. J. McGibbon, Interface Science **2**, 397, (1995).
[26] H. Kurata and C. Colliex, Phys. Rev. B **48**, 2102 (1993).
[27] G. Duscher, N. D. Browning, and S. J. Pennycook, in preparation.
[28] A. J. Craven and C. Colliex, J. Micr. Spectr. Elect. **2**, 511 (1977).
[29] G. Dehm, C. Scheu, G. Möbus, R. Brydson, and M. Rühle, Ultramicroscopy **67**, 207 (1997).
[30] S. J. Pennycook and D. E. Jesson, Ultramicroscopy **37**, 14 (1991).